Remote plasmon-induced heat transfer probed by the electronic transport of a gold nanowire

M.-M. Mennemanteuil, M. Buret, N. Cazier, G. Colas-Des-Francs, and A. Bouhelier
Laboratoire Interdisciplinaire Carnot de bourgogne, CNRS-UMR 6303,
Université Bourgogne Franche-Comté, 21078 Dijon, France

M. Besbes and P. Ben-Abdallah
Laboratoire Charles Fabry, Institut d'Optique Graduate School, CNRS,
Université Paris-Saclay, 91127 Palaiseau, France

(Received 9 March 2016; revised manuscript received 14 June 2016; published 11 July 2016)

We show in this paper that the heat generated by the optical excitation of resonant plasmonic antennas and diffusing along a simple glass/air interface disturbs the electron transport of a nearby conductive element. By probing the temperature-dependent resistance of a gold nanowire $R_{nw}(T)$, we quantitatively analyze the impact of a resonant absorption of the laser by the antennas. We find that the temperature rise at the nanowire induced by the laser absorption of a distant nanoparticle may exceed that of a direct illumination of the nanowire itself. We also find that a global calibration of the temperature-dependent resistance underestimates the heat generated locally by the laser. The local temperatures deduced from resistance variations are verified by numerical simulations with a very satisfactory agreement.

DOI: 10.1103/PhysRevB.94.035413

I. INTRODUCTION

The enhanced optical interaction cross sections brought by exciting surface plasmons on metal nanostructures play a central role for improving the emission characteristics of light-emitting devices [1] and are at the core of highly sensitive nanoscale biosensors [2–4]. The use of surface plasmons as a technological asset is also gaining ground in other applied research areas. For instance, the unique properties of surface plasmons are favorably employed to develop novel optoelectronic components [5–8] or to engineer thermal landscapes [9–12].

In this context, heat resulting from the resonant absorption of an incident radiation at the plasmon frequency may be exploited in photothermal cancer therapy [13,14] or may be applied to initiate local catalytic reactions [9,12,15]. A quantitative measurement of the local elevation of the temperature is typically obtained by measuring the subtle change of the refractive index of the surrounding medium [16], the anisotropy of polarization of a fluorescent species [17], or its temperature-dependent lifetime [18]. These measurements rely on a medium embedding the nanoheaters, and an estimation of the temperature is restricted to a few hundreds of nanometer corresponding to the water or polymer shell surrounding the nanoparticles [19–21]. Alternative measurement approaches rely on integrated bolometric and thermocouple devices for probing the temperature at the nanoscale [22–24]. The temperature elevations inferred from these investigations suggest that the thermal relaxation to the substrate is a factor that should not be neglected [25–27], in particular when operating plasmonic optoelectrical components in direct contact with an interface. In this case, the heat generated by the optical pumping of an electrically connected plasmonic device may disturb its current flow by increasing the device's resistance [24] and may be the source of undesired thermovoltages [6,28,29].

In this paper, we investigate the impact of a remote plasmon-induced heating on the electronic transport of a Au nanowire. By probing the change of resistance of the nanowire, we quantify the local temperature variation resulting from the optical absorption of distant illuminated Au nanodisks. We find that for a resonant photothermal excitation, the transport property of the nanowire is affected by the heat produced from irradiated nanodisks displaced as far as 6 μm away. We also find that the temperature rise at the nanowire induced by the optical pumping of a remote nanoheater may exceed that of a direct illumination of the nanowire itself.

II. EXPERIMENTAL METHODS

A. Nanofabrication

Figure 1(a) shows a scanning electron micrograph of a typical sample used in this work. It consists of four macroscopic electrodes connecting a nanowire and a set of nanodisks. The gold nanowires and nanodisks are fabricated by electron beam lithography on a standard glass coverslip. The nanowire has a nominal length of 15 μm and a width of 75 nm. The nanodisks are placed adjacent to the nanowire with varying diameters ranging from 90 to 410 nm. The structures are constituted of a 5-nm-thick Cr adhesion layer and a 60-nm-thick gold layer, which are both deposited by thermal evaporation. The nanowire is electrically connected to a set of macroscopic Au electrodes produced by standard photolithography and thermal evaporation. The electrodes are used to measure the nanowire's resistance in a four-probe configuration. The nanowire and the nearby nanodisks are readily seen at the center of the image. Figure 1(b) is a closeup image of the nanodisks. At the bottom of the nanowire, we design nanodisks with increasing diameters from left to right, whereas at the top of the nanowire, the same set of diameters is randomly ordered. The center-to-center distance between the nanowire and the nanoparticle is constant at 1 μm. In principle, the disks could be fabricated closer to the nanowire. However, the imaging resolution of our microscope would limit our ability to heat the disks without heating directly the

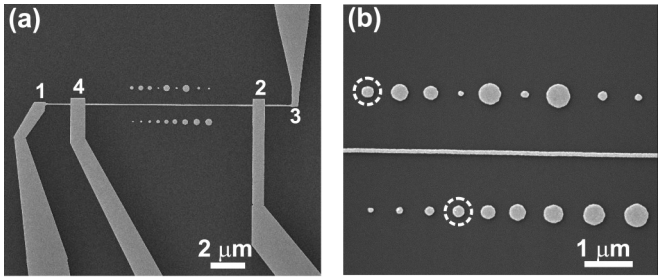

FIG. 1. (a) Scanning electron image of a contacted Au nanowire decorated by adjacent Au nanodisks in a four-probe resistance measurement. (b) Closeup image of the gold nanodisks placed nearby the nanowire. At the upper row, the diameters of the nanodisk are randomly arranged. At the bottom row, the diameters are increasing from left to right. The circled nanodisks are resonant with the laser wavelength.

nanowire. Furthermore, the absorption cross section of the nanodisks would be affected by the nanowire itself. For the same reasons, the interparticle edge separation is 500 nm to avoid short-range mutual coupling. The nanodisks are placed over a restricted distance of 5 μm with respect to the center of the nanowire to mitigate the influence of the large contact electrodes on the local temperature perceived by the nanowire. We found that for irradiated nanodisks placed too close to the electrical contacts, the latter act as efficient heat sinks. Thus, the transport response measured at the nanowire would differ between an optically pumped nanodisk positioned nearby the center of the nanowire and the same illuminated nanodisk placed in the vicinity of a large contact.

B. Electrical measurements

We use the following procedure to measure the electrical properties of the Au nanowire. A function generator (Française d'instrumentation) produces an ac voltage applied across the nanowire with an amplitude $V_{\rm ac} = 20$ mV and a frequency $F = 12.6$ kHz. This frequency is used as an external reference for a lock-in amplifier (UHFLI, Zurich Instrument). A current-to-voltage converter (DLPCA-200, Femto GmbH) detects the current flowing through the device, and the voltage output is sent to the lock-in amplifier as shown in Fig. 2. The output of the lock-in provides a voltage signal proportional to the amplitude of the modulated current oscillating at F. The differential resistance of the nanowire $R_{\rm nw}$ is then estimated by normalizing $V_{\rm ac}$ by the lock-in signal. For the sake of simplicity, we drop the term differential resistance in the remaining of the paper to simply refer to the resistance of the nanowire. We perform a four-probe measurement [30–32] to remove the contributions of the macroscopic electrodes and their contacts in the estimation of the nanowire resistance $R_{\rm nw}$. The parasitic resistances are successively evaluated by applying the ac voltage V_{ij} to each pair of electrodes and we measure the corresponding lock-in output signals. $i, j = 1$ to 4 are the contact labels, as defined in Fig. 1(a). The partial resistance of the sole nanowire writes $R_{L_{ij}}$, where L_{ij} is the distance between the electrode labeled i and the electrode labeled j. The contact resistance of each electrodes is R_i^c. The total resistance is thus $R_{ij} = R_i^c + R_j^c + R_{L_{ij}}$. The

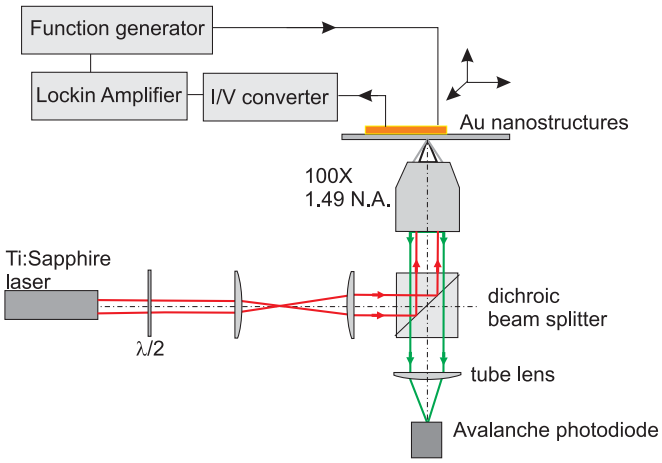

FIG. 2. Sketch of the experimental setup. The sample is scanned in the focus of a pulsed laser emitting 180-fs pulses with a repetition rate of 80 MHz centered at a wavelength of 810 nm. The nonlinear optical response (two-photon luminescence) is detected by an avalanche photodiode. The influence of the optical excitation on the electronic transport of the nanowire is recorded by a current-to-voltage converter feeding a lock-in amplifier. The lock-in amplifier is synced to the frequency of the ac bias applied to the nanowire by the function generator.

measurement follows the sequence below:

$$R_{13} = \frac{V_{13}}{I_{13}}, \quad R_{23} = \frac{V_{23}}{I_{23}},$$
$$R_{14} = \frac{V_{14}}{I_{14}}, \quad R_{24} = \frac{V_{24}}{I_{24}}. \tag{1}$$

With this procedure, we estimate the resistance of the nanowire $R_{\rm nw} = R_{L_{24}}$ corresponding to the central portion of the nanowire without the contact contributions using the relation [31]

$$R_{\rm nw} = \frac{(R_{13} - R_{14}) + (R_{24} - R_{23})}{2}. \tag{2}$$

For the nanowires fabricated in this work, the resistance may vary between processed samples. Otherwise noted, the nanowire considered in the following has a resistance $R_{\rm nw} = 175\ \Omega$, which corresponds to a metal resistivity for the evaporated Cr and Au layers of $\rho = R_{\rm nw} \times L_{\rm nw}/S = 6.5\ \mu\Omega$ cm, where S is the section of the nanowire. This value is consistent with the gold's resistivity reported from mesoscopic structures [33].

During the optical measurements discussed below, the bias $V_{\rm ac}$ is applied across the contacts labeled 1 and 3 in a two-probe configuration. The resistance R estimated from the output of the lock-in amplifier is then equal to the sum of the resistance of the two unknown electrical contacts R_1^c and R_3^c and the resistances $R_{L_{14}}$, $R_{\rm nw}$, and $R_{L_{23}}$ corresponding to the relevant portions of the nanowire. Assuming a constant resistivity ρ,

$$\begin{aligned} R &= R_{13} \\ &= R_1^c + R_3^c + R_{L_{14}} + R_{\rm nw} + R_{L_{23}} \\ &= R_1^c + R_3^c + \frac{\rho}{S}(L_{14} + L_{23}) + R_{\rm nw}. \end{aligned} \tag{3}$$

L_{14} and L_{23} are the lengths between the contacts 1–4 and 2–3, respectively. Knowing the resistance of the nanowire $R_{nw} = 175\ \Omega$ [Eq. (2)], the normalized output of the lock-in R_{13} and $\rho(L_{14} + L_{23})/S = 63\ \Omega$, the resistance of the contacts can be inferred to $R_1^c + R_3^c = 409\ \Omega$. The total contribution of the connections to the resistance amounts to 472 Ω. This value is subtracted from the resistance estimated from the two-probe lock-in measurement.

C. Local optical heating of the gold nanodisks

Figure 2 shows a schematic of the setup used in this study. The nanodisks are excited by a tightly focused Ti:sapphire laser beam emitting 180-fs pulses at a repetition rate of 80 MHz (Chameleon, Coherent). The wavelength is kept constant at 810 nm. The sample is placed on an inverted optical microscope (Eclipse, Nikon) equipped with a two-axis piezoelectric actuator (NanoLP-100, MadCity Labs) raster scanning the sample in the focal region. A 100× objective with a numerical aperture of 1.49 focuses the laser beam in a diffraction-limited spot and collects the nonlinear two-photon luminescence produced by the Au nanostructures [34,35]. The nonlinear signal is detected by an avalanche photodiode (Excelitas). The luminescence is used for imaging and analysis purposes. The average laser intensity at the sample is 420 kW cm^{-2} and the polarization of the focused laser beam is linearly polarized perpendicularly to the nanowire in order to homogenize the response along the object. We verified that the conclusions described below do not depend on the use of a pulsed laser. Leaving aside the nonlinear luminescent activity, similar results were consistently obtained for a constant-wave laser of the same power and emitting at 785 nm.

The basic picture of the physical mechanisms at play in the experiment can be summarized as follows: Upon local illumination of the nanodisks, the absorbed energy is converted to heat. Heat then dissipates by various decay channels including diffusion through the substrate and may thus reach the nanowire. The amount of heat perceived by the distant nanowire induces a drop of the electronic transport, which depends linearly on the nanowire temperature [36]. In the experiment, the change of resistance, that is the change of the transport properties, and the nonlinear signal emitted by the structures are simultaneously recorded for each position of the sample in the focus of the laser. The maps depicted in Fig. 3 are reconstructed images showing the variations of these two signals for each sample position. In Fig. 3(a), an increase of the resistance of the nanowire R_{nw} is clearly observed when the metal structures are optically excited. The contrast is constant when the laser is directly impinging the nanowire with a modest increase of its resistance. However, when the nanodisks are scanned through the focus, the variation of the nanowire's resistance ΔR_{nw} becomes dependent on the diameter of the nanodisks. Variations of ΔR_{nw} up to 1.4% are recorded for the ∼210 nm nanodisks as indicated by the arrows. These nanodisks are the elements circled in Fig. 1(b). For nearly all investigated diameters, the variation of the nanowire's resistance is larger when the laser irradiates the isolated nanodisks than for a direct illumination of the nanowire itself.

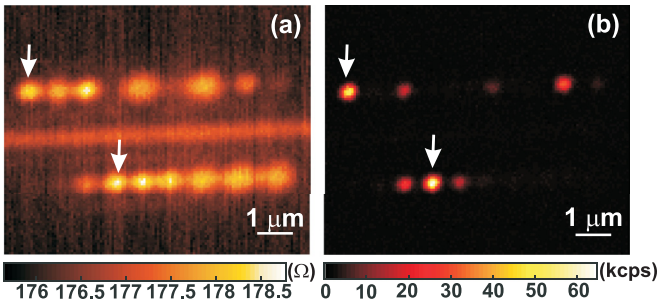

FIG. 3. (a) Two-dimensional map of the nanowire's resistance R_{nw} for a lateral scan of the sample in the focal spot of the laser. Heat generated by the laser on the different metal parts of the sample provides an increase of the nanowire's resistance. (b) Simultaneously acquired nonlinear two-photon luminescence emitted by the Au structures. The nanodisks in resonance with the laser (arrows) are inducing the largest variation of the resistance and the strongest nonlinear photoluminescence.

Heat generated during the optical excitation of the nanodisks depends directly on their absorbing capacity, which is enhanced at the surface plasmon resonance. The occurrence of the resonance is readily identified in the nonlinear two-photon luminescence produced by the nanodisks [35,37] as illustrated in the confocal map of Fig. 3(b). The strongest response is observed for the 210-nm nanodisk (arrows). The red curve in Fig. 4(a) shows the nonlinear photoluminescence dependence with the size of the nanodisks obtained from three different samples. At the laser wavelength used in this study, the ∼210 nm nanodisk sustains a marked resonance. The largest ΔR_{nw} in Fig. 3(a) is also observed for this diameter.

The resonance is numerically confirmed by simulating the absorption cross section σ_a of a nanodisk as a function of its diameter. The absorption cross section of the Au nanodisk writes

$$\sigma_a(\omega) = \frac{P_a(\omega)}{\psi_i(\omega)}. \tag{4}$$

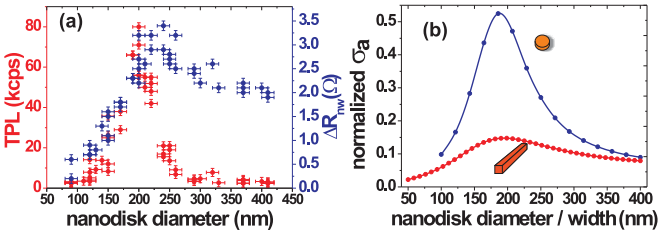

FIG. 4. (a) Evolution of the variation of the resistance ΔR_{nw} and the two-photon luminescence (TPL) with nanodisk diameter. A plasmon resonance is clearly identified for nanodisks with a diameter of 210 nm. The graph gathers measurements obtained from three different samples. (b) Blue curve: simulated evolution of the absorption efficiency of a Au nanodisk placed on a glass substrate as a function of its diameter. The simulated resonant absorption occurs for ∼200 nm nanodisk. Red curve: absorption efficiency for a nanowire as a function of its width. The polarization is perpendicular to the main axis of the nanowire.

$\sigma_a(\omega)$ is defined for an incident monochromatic plane wave of frequency ω as the ratio of the absorbed power

$$P_a(\omega) = \frac{\omega}{2}\int_v |E|^2 \mathrm{Im}(\varepsilon) dV \tag{5}$$

by the incident flux

$$\psi_i(\omega) = \frac{1}{2}\left(\frac{\epsilon_0}{\mu_0}\right)^{1/2} |E|^2. \tag{6}$$

Here, ε denotes the electric permittivity of the absorber of volume V, E is the local electric field, and ϵ_0 and μ_0 are the vacuum permittivity and permeability, respectively. The absorption cross sections of the nanodisks and of the nanowire are calculated by solving Maxwell's equations with a finite-element method combined to an analytical description of the field scattered at the interface of the substrate [38]. The absorption cross section is represented by the blue curve in Fig. 4(b) after a normalization by the surface of the absorbers. The presence of the glass substrate is taken into account in the calculations. The simulation clearly indicates an enhanced absorption efficiency for a particle diameter ~200 nm. The red curve in Fig. 4(b) is the calculated absorption efficiency for a nanowire with varying widths. The structure is assumed invariant along the nanowire axis and the calculation is performed for a linear polarization aligned with the short axis. For the experimental width investigated in this work (75 nm), σ_a for the nanowire is ~5 times weaker than for a resonant nanodisk. This agrees well the experimental resistance's map of Fig. 3(a). The contrast is dimmer for a direct illumination of the nanowire compared to resonant disks despite the fact that they are laterally shifted by 1 μm. These consistent results confirm the unambiguous role of the surface plasmon resonance at generating an absorption enhancement and the subsequent rise of the temperature-dependent resistance of the nanowire [24].

Interestingly, the variation of the resistance with the nanodisk diameter follows a different trend than the nonlinear photoluminescence as illustrated by the blue curve in Fig. 4(a). ΔR_{nw} increases to reach a maximum at 3.5 Ω for ~220 nm nanodisks and then reduces to reach a plateau at 2 Ω for diameters larger than 350 nm. This threshold diameter corresponds to the approximate size of the focal spot. The evolution of ΔR_{nw} is thus the convolution of a profile related to the plasmon resonance with a size dependence related to the saturation of the optical absorption for nanodisks larger than the focal spot.

We verified numerically that mutual interactions between adjacent nanodisks can be neglected with the interparticle distance considered in this work. Figure 5 describes the evolution of the optical absorption σ_a of an excited nanodisk in the presence of a second gold nanodisk of the same size placed at a distance d from the first, and that for two crossed polarizations. Interestingly, the calculations predict that the optical absorption of a nanodisk can be dressed by adjusting either of the three parameters. The dashed line is the edge-to-edge distance used in the experiment. At 500-nm distance between the nanodisks, the optical absorption of a unit is not disturbed by the presence of the second one even when excited at resonance. This is implicitly shown in the resistance map of Fig. 3(a) where the variation of the resistance for a given nanodisk placed above or below the nanowire is the same regardless of its immediate adjacent environment.

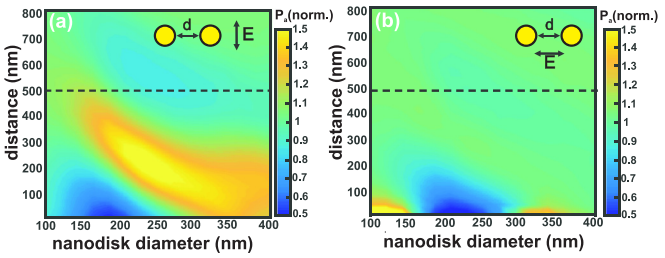

FIG. 5. (a), (b) Dependence of the power absorbed P_a inside one nanodisk in the presence of a second one for varying edge-to-edge distances d and disk diameters. The maps are calculated for a TE polarization and a TM polarization, respectively. The absorbed power is normalized to the absorption of a single isolated nanodisk. Therefore, when the nanodisks are uncoupled, P_a is equal to 1. The excitation is a plane wave normally incident to the interface with a wavelength $\lambda = 810$ nm. The dashed line corresponds the minimum experimental distance between the nanodisks in Fig. 1 confirming the negligible mutual interaction between the nanodisks.

D. Temperature calibration

In order to estimate the rise of the nanowire's temperature, we calibrate the temperature-dependent resistance of the nanowire $R_{\mathrm{nw}}(T)$ by placing the sample on a controlled heating module in line with the reports by Herzog and co-workers [24] and Stolz *et al.* [6]. Briefly, the entire sample is placed on a Peltier element powered by a regulated power supply. The thermal transfer between the heating element and the glass substrate is ensured by a thin layer of a thermal grease. A thermocouple in contact with the sample monitors the global voltage-controlled temperature of the device. A sketch of the apparatus is depicted in the inset of Fig. 6(a). For calibrating the temperature-dependent resistance of the nanowire, we measure ΔR_{nw} for a series of temperature T_{global} heating the entire sample above room temperature. The increase of ΔR_{nw} with temperature is displayed in Fig. 6(a). The data are fitted with a linear regression with a slope $d\Delta R_{\mathrm{nw}}/dT_{\mathrm{global}} = 0.41\ \Omega\,\mathrm{K}^{-1}$. This value depends on the resistivity of the nanowire and its characteristic dimensions. The variation ΔR_{nw} recorded during the lateral scan of the nanowire in the focal spot [Fig. 3(a)] may be linked to a first approximation to the temperature deviation from room temperature $\Delta T_{\mathrm{global}}$. Because the sample is heated homogeneously, the change of temperature at the nanowire $\Delta T_{\mathrm{nw}}^{\mathrm{global}}$ equals that of the entire sample $\Delta T_{\mathrm{nw}}^{\mathrm{global}} = \Delta T_{\mathrm{global}}$. The black curve in Fig. 6(b) is the inferred temperature elevation of the nanowire $\Delta T_{\mathrm{nw}}^{\mathrm{global}} = 2.3$ K considering the rise of resistance ΔR_{nw} measured in Fig. 3(a) when the laser irradiates directly the nanowire.

The temperature deduced by this procedure is valid for a nanowire heated homogeneously over its length. This approximation is, however, not representative of a local excitation of the nanowire by a tightly focused laser beam. In this case, a temperature gradient exists and the calibration performed by a global warming of the sample is no longer

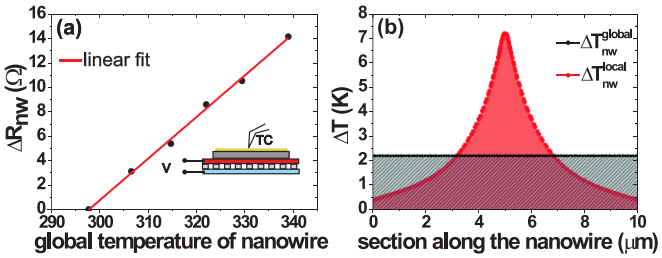

FIG. 6. (a) Evolution of nanowire resistance $R_{\rm nw}$ with a global increase of the sample temperature. The entire sample is heated above room temperature with a voltage-controlled Peltier module as sketched in the inset. A thermocouple (TC) records the temperature at the sample's surface for a series of voltage-controlled (V) settings applied to the Peltier module. The block scheme for measuring the resistance is omitted for clarity and is the same as in Fig. 2. (b) Black curve: constant temperature along the nanowire estimated from the $dR_{\rm nw}/dT_{\rm global}$ coefficient deduced from (a) and the $\Delta R_{\rm nw}$ recorded by the lock-in amplifier during laser illumination. Red curve: simulated distribution of the temperature along the nanowire for a local heating element centered on the nanowire. The maximum temperature is computed to set the area under the red curve equal to that under the black curve.

appropriate. To motivate this point, we show in Fig. 6(b) a finite-element simulation (COMSOL multiphysics) of the longitudinal distribution of $\Delta T_{\rm nw}^{\rm local}$ produced by a simulated heat source located at the center of the nanowire and with a dimension corresponding to the focal spot. To estimate the local temperature of the heat source, we equalize the resistance variation due to a homogeneous heating with a rise of temperature $\Delta T_{\rm nw}^{\rm global}$ using the Peltier module and the resistance change by a local heating with a temperature $\Delta T_{\rm nw}^{\rm local}(x)$. x is the coordinate along the nanowire length $L_{\rm nw}$. For a temperature-dependent resistivity $\rho(T)$, this equality writes

$$\Delta R_{\rm nw} = \frac{\rho\left(\Delta T_{\rm nw}^{\rm global}\right) L_{\rm nw}}{S} = \int_0^{L_{\rm nw}} \frac{\rho\left[\Delta T_{\rm nw}^{\rm local}(x)\right]}{S} dx. \quad (7)$$

From the linear relationship between $R_{\rm nw}$ and $T_{\rm nw}^{\rm global}$ depicted in Fig. 6(a), Eq. (7) is satisfied if the areas under the profiles $\Delta T_{\rm nw}^{\rm local}(x)$ and $\Delta T_{\rm nw}^{\rm global}(x)$ along the nanowire are equal. We thus compute the maximum local temperature $\Delta T_{\rm nw}^{\rm local,max}$ to satisfy the equality. In Fig. 6(b), we set $\Delta T_{\rm nw}^{\rm local,max} = 7.2$ K to have identical areas under the two curves. For the same change of resistance, the maximum temperature reached by the nanowire $\Delta T_{\rm nw}^{\rm local,max}$ is thus three times higher for a diffraction-limited local heat source than for a global heating of the system. This approach is valid for a local heating of the nanowire, but would fail at describing a situation where a local rise of the temperature would be compensated by a local cooling of the system. In this particular case, $R_{\rm nw}$ would remain unchanged.

The geometry of the nanowire and of the nanodisks used in the computation are taken from the experimental structures without the adhesion layer. Two 500 nm × 20 μm gold pads mimicking the electrodes are placed at the extremities of the nanowire. The nanowire, the nanodisks, and the pads are deposited on a 50 μm × 50 μm × 50 μm cube of glass. The material properties used in the calculations are for the thermal capacity: $C^{\rm Au} = 129\ {\rm J\,kg^{-1}\,K^{-1}}$ and $C^{\rm glass} = 730\ {\rm J\,kg^{-1}\,K^{-1}}$; for the thermal conductivity: $\kappa^{\rm Au} = 317\ {\rm W\,m^{-1}\,K^{-1}}$ and $\kappa^{\rm glass} = 1.4\ {\rm W\,m^{-1}\,K^{-1}}$; and for the electrical conductivity: $\sigma^{\rm Au} = 45.6 \times 10^6\ {\rm S\,m^{-1}}$ and $\sigma^{\rm glass} = 1 \times 10^{-14}\ {\rm S\,m^{-1}}$. The initial temperature at the boundaries of the calculation window is 296.15 K. The surface emissivity for Au is $\epsilon^{\rm Au} = 0.02$, and for glass $\epsilon^{\rm glass} = 0.94$. The system is considered at equilibrium, that is, the temperature does not evolve with time. The simulation takes into account the radiative contribution to the heat transfer. However, for the temperature range of the nanowire investigated here, Cheng *et al.* demonstrated that radiation loss may be neglected [39]. Energy dissipated to the air medium by radiation and convection may become dominant over to the energy lost in the substrate for very specific conditions (high pressure, small nanowire decoupled from the substrate). Our experimental and computational conditions differ from this restrictive regime.

The approach described above is applied to estimate the temperature distribution along the nanowire for a laser excitation of the gold nanodisks. Under this configuration heat must diffuse through the substrate to impact the nanowire's resistance. An example of the procedure is shown in Fig. 7(a) for the resonant disk identified in the $\Delta R_{\rm nw}$ map of Fig. 3(a). The curve is simulated using the following steps. We first determine the experimental value $\Delta R_{\rm nw}$ of the nanowire when the nanodisk is irradiated. For the case considered here $\Delta R_{\rm nw} = 2.8\ \Omega$. Using the global temperature coefficient $dR_{\rm nw}/dT_{\rm global} = 0.41\ \Omega\,{\rm K^{-1}}$, we estimate what would be the necessary global temperature change required to increase the resistance by 2.8 Ω, that is, $\Delta T_{\rm global} = 6.9$ K. This hypothetical temperature is homogeneously distributed along the nanowire [dashed curve in Fig. 7(a)]. To take into account the local illumination of the nanodisk by the focused laser beam, we compute the two-dimensional distribution of the temperature in the system considering a heated nanodisk [see inset in Fig. 7(a)]. We then take a profile of the temperature reached along the nanowire as illustrated by the red curve in Fig. 7(a). We adjust the temperature of the heat source in the finite-element simulation of the system to obtain equal areas under the two temperature profiles perceived by the nanowire. For

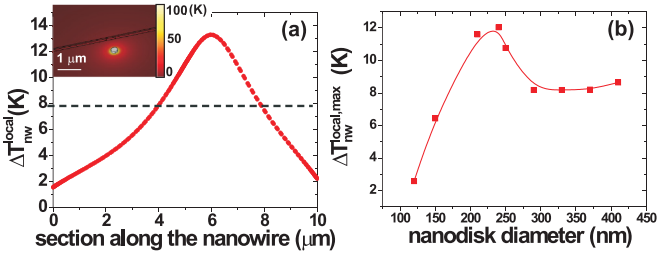

FIG. 7. (a) Estimated temperature gradient along the nanowire when a 210-nm-diameter nanodisk is heated at a distance of 1 μm and introduces a 2.8 Ω rise of the nanowire's resistance. Dashed line: global temperature required to change the resistance by the same amount. Inset: spatial distribution of the simulated temperature in the computed system. (b) Maximum temperature deduced from the experimental variation of the nanowire's resistance as a function of the nanodisk's diameter.

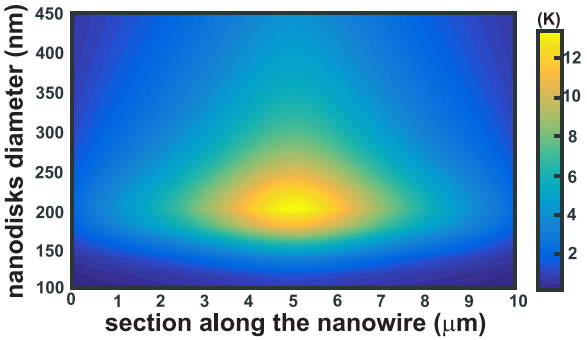

FIG. 8. Computed temperature variation along the nanowire for varying nanodisk diameters placed at a distance of 1 μm. The nanodisks are the source of heat. The graph is calculated by a finite-element analysis taking into account the experimental conditions (focused beam, incident power, and size of the structures).

a temperature rise of the nanodisk of 108 K, the surfaces under the two curves in Fig. 7(a) are identical. The maximum temperature rise at the nanowire is about $\Delta T_{\rm nw}^{\rm local,max} = 13$ K. Conducting this analysis for the range of diameters considered in this study, we show in Fig. 7(b) that $\Delta T_{\rm nw}^{\rm local,max}$ remains significant even for optically pumped nanodisks laterally shifted by 1 μm.

In the following, we estimate the rise of the temperature in the nanowire purely from a simulation standpoint. The objective is to verify the reliability of the temperature variations deduced from the approach outlined by Eq. (7). To do so, the problem is solved by a finite-element analysis of the combined physical processes at play. The temperature of the nanodisk is no longer derived from the variation of the nanowire's resistance. It is directly computed from the electromagnetic problem consisting at calculating the power absorbed by the Au nanodisks upon illumination of a simulated focused beam.

We compute the steady-state longitudinal distribution of the temperature along the nanowire for the different nanodisks considered experimentally. The results are reported in Fig. 8. The highest computed temperature variation $\Delta T_{\rm nw}^{\rm local,max} = 12$ K is in very good agreement with the temperature determined from transport measurement [Fig. 7(b)]. Furthermore, the full calculation reproduces the plateau observed for large diameters in Fig. 7(b). These similarities demonstrate the consistency of the resistance analysis used to deduce the local elevation of the temperature $\Delta T_{\rm nw}^{\rm local,max}$.

For diameters exceeding the size of the laser beam, the simulated $\Delta T_{\rm nw}^{\rm local,max}$ is a factor 2 lower than the experimentally inferred value. The profile of the temperature along the nanowire used for the calculation of $\Delta T_{\rm nw}^{\rm local,max}$ is obtained by the diffusion of a homogeneous heat source through the glass substrate. This approximation is correct when the plasmonic nanodisk is smaller than the laser beam. For larger diameters, the optical excitation of nanodisk can no longer be approximated to a homogeneous heat source and is the probable source of the discrepancy.

III. LONG-RANGE HEAT TRANSFER

Thus far, we considered illuminated nanodisks laterally displaced by 1 μm from the nanowire. For the laser intensity

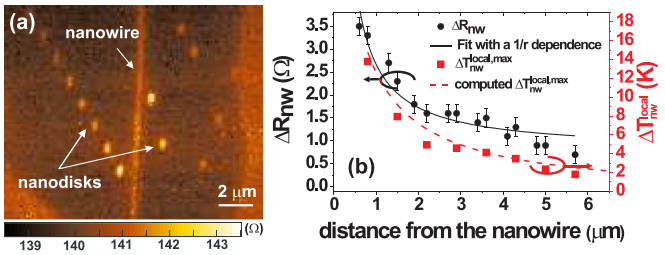

FIG. 9. (a) Two-dimensional map of the nanowire's resistance when the structure is scanned through the focus. The resistance increases whenever the laser is heating the nanostructures in the scanned area. On the left side of the nanowire, the distance of the resonant nanodisks is increasing stepwise. On the right side, nanodisks are randomly shifted from the nanowire. (b) Left axis: (circle) variation of the nanowire's resistance $\Delta R_{\rm nw}$ as a function of the distance between the nanodisks and the nanowire. Solid black line: best fit to the experimental data points considering a $1/r$ distance dependence, where r is the distance between the heat source and the nanowire. The characteristic decay length is 1.8 μm. Right axis: (square) estimated variation of the maximum temperature perceived by the nanowire. Red dashed line: computed maximum variation of the temperature.

used, the temperature at the nanodisk reaches 108 K for a resonant structure. At the shifted position of the nanowire, we estimated the temperature elevation of 13 K. In the following, we investigate the distance dependence of the heat transfer via the glass substrate.

In this experiment, we place resonant nanodisks at distances from the nanowire ranging from 800 nm to 6 μm. The study is conducted on a nanowire with a resistance $R_{\rm nw} = 138\ \Omega$ and we maintain constant the optical conditions. Figure 9(a) is a two-dimensional distribution of the resistance $R_{\rm nw}$ when the sample is laterally scanned through the focus. On the left side of the nanowire, the separation between the nanodisks and the nanowire increases from bottom to top. On the right side of the nanowire, the distances are randomly ordered. We observe the same contrast as in Fig. 3(a) with an increase of the nanowire's resistance when the Au structures are heated by the laser. We plot on the left axis of Fig. 9(b) the variation of the resistance $\Delta R_{\rm nw}$ as a function of the lateral displacement of the nanodisks. The heat generated by the laser incident on a nanodisk remotely placed as far as 6 μm and diffusing through the glass substrate imparts a measurable rise of the nanowire resistance. Formally, the temperature of a pointlike source in a three-dimensional system evolves as $C/r \times \mathrm{erf}[r/\sqrt{4Dt}]$ where D is the diffusivity of the material, C is a constant that depends on the power which is dissipated by the source, and r is the distance to the source and erf is the error function [40]. When t becomes large enough (steady-state regime), the temperature varies as $1/r$, which is analog to the field generated in far-field regime by a local dipole. The fit to the data with a $1/r$ dependence provides a decaying diffusion with a characteristic length of 1.8 μm.

Following the procedure described above, we calculate the maximum temperature variation $\Delta T_{\rm nw}^{\rm local,max}$ via the calibration coefficient $dR_{\rm nw}/dT_{\rm global}$ determined by a global heating [Fig. 6(a)] and the spatial distribution of temperature

determined by the finite-element analysis [Fig. 7(a)]. The maximum temperature $\Delta T_{nw}^{local,max}$ is plotted in the right axis of Fig. 9(b). At a distance of 800 nm from the nanowire, the excitation of a resonant structure raises the nanowire's temperature by about 14 K. For the same nanodisk placed at 6 μm, $\Delta T_{nw}^{local,max}$ drops to 2 K. The red curve is the calculated $\Delta T_{nw}^{local,max}$ using the full computation and is in very good agreement with the points (square) deduced from the experimental ΔR_{nw}.

IV. CONCLUSIONS

We have investigated the effect of a remote resonant plasmonic photothermal excitation on the electronic transport of a Au nanowire. Upon focusing light on isolated Au nanodisks, the heat locally produced diffuses through the substrate and induces a change of the nanowire's resistance. We deduce the temperature rise at the nanowire by taking into account the local nature of the excitation, the experimental data, and finite-element calculations. We estimate a local temperature rise at the nanowire of 13 K for a laser intensity of 420 kW cm^{-2} focused on a resonant plasmonic nanoparticle located 1 μm away from the nanowire. The photothermal excitation of an electrically contacted metal nanowire resting on a glass surface is usually considered negligible. While the macroscopic electrodes connected to the nanowire act as heat sinks and the physical contact to the substrate contributes to an efficient cooling of the nanowire by thermal conduction [41], we determine a maximum temperature exceeding the average temperature inferred from a global calibration of the temperature-dependent resistivity of the nanowire [5,6,24]. Interestingly, we demonstrate that the rise of temperature for a direct optical excitation of the nanowire is weaker than for a laterally displaced isolated resonant nanoparticle. The thermal diffusion through the glass substrate follows a decay of about 1.8 μm, and illuminated nanodisks located as far as 6 μm generate a temperature variation of 2 K at the nanowire. While all the experiments are conducted in the steady-state regime, the protocol can be readily extended to a time-dependent thermoplasmonic modulation [42] of the electronic transport of the nanowire.

To conclude, we demonstrate that relatively simple electrical measurements can be implemented to remotely probe the plasmon-induced photothermal activity of an illuminated device. By extension, measuring the resistance variations of a network of such heat probes may enable a diffusion-based thermal tomography of a local heat source. We believe that thermal diffusion through the substrate may be mitigated or conversely enhanced by a careful control of the electromagnetic interaction between an ensemble of nanoparticles. In line with this concluding remark, a phononic engineering [43] of the substrate's local thermal conductivity would also offer a leverage to control the directional flow of the heat produced by the resonant absorption.

ACKNOWLEDGMENTS

The research leading to these results has received funding from the European Research Council under the European Community's Seventh Framework Program FP7/ 2007-2013 Grant Agreement No. 306772. This project is in cooperation with the Labex ACTION (Contract No. ANR-11-LABX-01-01) and the regional PARI programs. The authors are grateful to O. Demichel for valuable discussions.

[1] C.-Y. Cho, S.-J. Lee, J.-H. Song, S.-H. Hong, S.-M. Lee, Y.-H. Cho, and S.-J. Park, Appl. Phys. Lett. **98**, 051106 (2011).
[2] G. J. Nusz, S. M. Marinakos, A. C. Curry, A. Dahlin, F. Höök, A. Wax, and A. Chilkoti, Anal. Chem. **80**, 984 (2008).
[3] S. K. Dondapati, T. K. Sau, C. Hrelescu, T. A. Klar, F. D. Stefani, and J. Feldmann, ACS Nano **4**, 6318 (2010).
[4] J. Nyagilo, S.-H. Chang, J. Wu, Y. Hao, and D. P. Davé, Sens. Actu. B: Chem. **212**, 225 (2015).
[5] D. R. Ward, F. Hüser, F. Pauly, J. C. Cuevas, and D. Natelson, Nat. Nanotechnol. **5**, 732 (2010).
[6] A. Stolz, J. Berthelot, M.-M. Mennemanteuil, G. Colas des Francs, L. Markey, V. Meunier, and A. Bouhelier, Nano Lett. **14**, 2330 (2014).
[7] M. L. Brongersma, N. J. Halas, and P. Nordlander, Nat. Nanotechnol. **10**, 25 (2015).
[8] A. Melikyan, L. Alloatti, A. Muslija, D. Hillerkuss, J. L. P. C. Schindler, R. Palmer, D. Korn, S. Muehlbrandt, D. V. Thourhout, B. Chen, R. Dinu, M. Sommer, C. Koos, M. Kohl, W. Freude, and J. Leuthold, Nat. Photonics **8**, 229 (2014).
[9] G. Baffou, C. Girard, and R. Quidant, Phys. Rev. Lett. **104**, 136805 (2010).
[10] A. Sanchot, G. Baffou, R. Marty, A. Arbouet, R. Quidant, C. Girard, and E. Dujardin, ACS Nano **6**, 3434 (2012).
[11] G. Baffou and R. Quidant, Laser Photon. Rev. **7**, 171 (2013).
[12] G. Baffou and R. Quidant, Chem. Soc. Rev. **43**, 3898 (2014).
[13] W. Chen, C. Ayala-Orozco, l. N. C. Biswa, C. Perez-Torres, M. Bartels, R. Bardhan, G. Stinnet, X. D. Liu, B. Ji, A. Deorukhkar, L. V. Brown, S. Guha, R. G. Pautler, S. Krishnan, N. J. Halas, and A. Joshi, Nanomedicine **9**, 1209 (2014).
[14] E. B. Dickerson, E. C. Dreaden, X. Huang, I. H. El-Sayed, H. Chu, S. Pushpanketh, J. F. McDonald, and M. a. El-Sayed, Cancer Lett. **269**, 57 (2008).
[15] S. Mukherjee, L. Zhou, A. M. Goodman, N. Large, C. Ayala-Orozco, Y. Zhang, P. Nordlander, and N. J. Halas, J. Am. Chem. Soc. **136**, 64 (2014).
[16] G. Baffou, P. Bon, J. Savatier, J. Polleux, M. Zhu, M. Merlin, H. Rigneault, and S. Monneret, ACS Nano **6**, 2452 (2012).
[17] G. Baffou, M. P. Kreuzer, F. Kulzer, and R. Quidant, Opt. Express **17**, 3291 (2009).
[18] Z. J. Coppens, W. Li, D. G. Walker, and J. G. Valentine, Nano Lett. **13**, 1023 (2013).
[19] V. Kotaidis and A. Plech, Appl. Phys. Lett. **87**, 213102 (2005).
[20] A. O. Govorov, W. Zhang, T. Skeini, H. Richardson, J. Lee, and N. A. Kotov, Nanoscale Res. Lett. **1**, 84 (2006).
[21] A. N. Volkov, C. Sevilla, and L. V. Zhigilei, Appl. Surf. Sci. **253**, 6394 (2007).
[22] E. Shapira, Marchak, and A. T. Y. Selzer, Nanotechnology **19**, 125501 (2008).

[23] J.-C. Weeber, K. Hassan, A. Bouhelier, G. Colas-des Francs, J. Arocas, L. Markey, and A. Dereux, Appl. Phys. Lett. **99**, 031113 (2011).
[24] J. B. Herzog, M. W. Knight, and D. Natelson, Nano Lett. **14**, 499 (2014)
[25] M. Tschikin, S.-A. Biehs, F. Rosa, and P. Ben-Abdallah, Eur. Phys. J. B **85**, 253 (2012).
[26] M. T. Carlson, A. J. Green, A. Khan, and H. H. Richardson, J. Phys. Chem. C **116**, 8798 (2012).
[27] M. Tzur, B. Desiatov, I. Goykhman, M. Grajower, and U. Levy, Opt. Express **21**, 29195 (2013).
[28] B. Y. Zheng, H. Zhao, A. Manjavacas, M. McClain, P. Nordlander, and N. J. Halas, Nat. Commun. **6**, 7797 (2015).
[29] F. Léonard, E. Song, Q. Li, B. Swartzentruber, J. A. Martinez, and G. T. Wang, Nano Lett. **15**, 8129 (2015).
[30] H. Okino, I. Matsuda, R. Hobara, Y. Hosomura, S. Hasegawa, and P. A. Bennett, Appl. Phys. Lett. **86**, 233108 (2005).
[31] W. Gu and K. Kim, in *IEEE Nanotechnology Materials and Devices Conference*, Vol. 1 (IEEE, Piscataway, NJ, 2006), p. 304.
[32] A. S. Walton, C. S. Allen, K. Critchley, M. L. Gorzny, J. E. McKendry, R. M. D. Brydson, B. J. Hickey, and S. D. Evans, Nanotechnology **18**, 065204 (2007).
[33] P. M. T. M. van Attekum, P. H. Woerlee, G. C. Verkade, and A. A. M. Hoeben, Phys. Rev. B **29**, 645 (1984).
[34] M. R. Beversluis, A. Bouhelier, and L. Novotny, Phys. Rev. B **68**, 115433 (2003).
[35] A. Bouhelier, R. Bachelot, G. Lerondel, S. Kostcheev, P. Royer, and G. P. Wiederrecht, Phys. Rev. Lett. **95**, 267405 (2005).
[36] A. Piróth and J. Sólyom, *Fundamentals of the Physics of Solids: Volume II: Electronic Properties*, Fundamentals of the Physics of Solids (Springer, Berlin, 2008).
[37] P. Ghenuche, S. Cherukulappurath, T. H. Taminiau, N. F. van Hulst, and R. Quidant, Phys. Rev. Lett. **101**, 116805 (2008).
[38] J.-M. Jin, *The Finite Element Method in Electromagnetics*, 3rd ed. (Wiley, Hoboken, NJ, 2014).
[39] C. Cheng, W. Fan, J. Cao, S.-G. Ryu, J. Ji, C. P. Grigoropoulos, and J. Wu, ACS Nano **5**, 10102 (2011).
[40] M. N. Ozisik, *Heat Conduction*, 3rd ed. (Wiley, New York, 2002).
[41] B. Kopp, Z. Yi, D. Benner, F. Q. Xie, C. Obermair, T. Schimmel, J. Boneberg, P. Leiderer, and E. Scheer, Beilstein J. Nanotechnol. **3**, 703 (2012).
[42] S. Dilhaire, G. Pernot, G. Calbris, J. M. Rampnoux, and S. Grauby, J. Appl. Phys. **110**, 114314 (2011).
[43] M. Maldovan, Nature (London) **503**, 209 (2013).